PLATE-TYPE ACOUSTIC METAMATERIALS

Fuyin Ma and Jiu Hui Wu

School of Mechanical Engineering and State Key Laboratory for Strength and Vibration of Mechanical Structure, Xi'an Jiaotong University, Xi'an, China
xjmafuyin@xjtu.edu.cn, and ejhwu@xjtu.edu.cn

Keywords: Plate-type acoustic metamaterials, Local resonance, Lightweight structure, Low frequency sound insulation

ABSTRACT

The experimental realization and theoretical understanding of ultrathin lightweight plate-type acoustic metamaterials structures have been presented and discussed in-depth, wherein broadband excellent sound attenuation ability at low frequencies is realized by employing locally resonant effect. Here three different design concepts of plate-type acoustic metamaterials were introduced as below: a) Based on square lattice plate-type acoustic metamaterials, firstly, by increasing the membrane thickness, dependence on the initial tension of the membrane has been reduced or even completely eliminated, then a plate-type acoustic metamaterial with outstanding low frequency broadband sound insulation performance are proposed, and the influence of film thickness on the insulation properties is realized; secondly, by employing the elastic plate structure without initial tension, locally resonant theory of the plate-type acoustic metamaterials are established, and the sound insulation properties are connected to the band structure; thirdly, the influence of the mass shape on band gap is revealed by locally resonant theory; b) By introducing a thin air layer between the films, a type of multilayer one-dimensional membrane and plate-type acoustic metamaterials structures with excellent low frequency sound insulation performance are experimentally obtained; c) Some plate-type acoustic metamaterial structures with lumped coupling bending resonance effects are experimentally and theoretically proposed, which have excellent low frequency ultra-wideband sound insulation ability, and even without any mass block, strong sound attenuation up to nearly 99% is experimentally achieved.

1 INTRODUCTION

Due to the low frequency sound wave with wavelength as long as from several meters to hundreds of meters, by using the traditional methods, the sound insulation structures need making the thickness size comparable with the wavelength for effectively isolating the wave. Theoretically, according to the mass density law, at low frequencies the acoustic transmission through a plate is inversely proportional to the thickness, mass density, and sound frequency [1]. That implies the low-frequency performance of barriers can be improved by increasing the thickness and ultimately the mass of the system [2]. However, in most cases this method is difficult for this to manipulate in practice due to the weight and volume constraints. So, the attenuation of low-frequency sound is a very challenging task [3]. The emergences of phononic crystals and acoustic metamaterials have provided a new thought for the vibration and noise attenuation at low frequencies. In 2000, the locally resonant phononic crystal had been put forward, wherein the cell size is two orders lower than the corresponding wavelength [4]. And that work has also been regarded as the origin of acoustic metamaterials [5]. Over the past decade, a great number of locally resonant phononic crystals and acoustic metamaterials structures with special functions were proposed [1-8]. Particularly, a membrane-type acoustic metamaterial with deep subwavelength thicknesses was proposed in 2008 [9], and provided a new solution for engineering vibration and noise reduction. By employing minimal rigidity of the elastic membrane, the low-frequency sound attenuation and other novel properties could be obtained [1-3, 9-20].

The previous proposed elastic membrane-type acoustic metamaterial structures have shown very excellent sound reflection or absorption abilities. However, on the one hand, the stability of acoustic performance in elastic membrane structure is poor, and the resonant frequency is sensitive to the membrane tension, where very slight tension difference could lead to a large frequency offset; on the

other hand, silicone rubber material has been widely used in the elastic membrane-type acoustic metamaterials, and such material very easily tends to aging even without external loads. In this paper, we given a scheme to reduce the tension dependence by increasing the membrane thickness for improving the stability of acoustical performance. Actually, the tension dependence feature can also be eliminated by using the materials with higher Young's modulus to replace the soft rubber. However, the rigidity of plates are several orders higher than that of soft rubber membranes, which makes the design of the locally resonant structures using the stiff plates for low frequency sound attenuation to be difficult. Therefore, we proposed a one-dimensional (1D) stiff film-type acoustic metamaterials by introducing the thin air layer between films for low frequency sound attenuation, in which the resonant frequencies of structures are sufficiently low and the difficulty of tension control vanishes. However, the sound attenuation abilities of 1D structure are not good enough, and the total thickness is also larger than that of two-dimensional (2D) elastic membrane-type acoustic metamaterials structure. Therefore, a type of 2D multiple cells lumped ultrathin lightweight plate-type acoustic metamaterials structure with excellent sound attenuation in the low frequency range is proposed. With excellent sound attenuation ability, the proposed metamaterials could initiate exciting possibilities for designing subwavelength thicknesses sound barriers with versatile potential, and the application of noise reduction could be extended to new fields, such as the vehicle and resident environment.

2 LOCALLY RESONANT PROPERTY OF 2D PLATE ACOUSTIC METAMATERIALS

We designed several types of typically square lattice localized resonance units by silicone rubber, EVA and ABS materials, which were shown in Fig. 1a~d. Each unit consists of three parts, namely mass block, plate and frame. The mass block and plate are constituted by flexible rubber, and the frame by flexible EVA or stiff ABS. Total four types of mass block are considered, that is, cylindrical, ring, rectangular, and hemispherical shapes. Due to the different shape of the mass, the anisotropy, symmetry and surface density of units appear different respectively, followed by the difference of band structures. We also fabricated the corresponding experimental samples, and part of the samples are shown in Fig. 1e~h, the detailed settings and parameters can be found in our previous works [10-11]. A homogeneous EVA plate with thickness of 2.5mm is chosen as the control group.

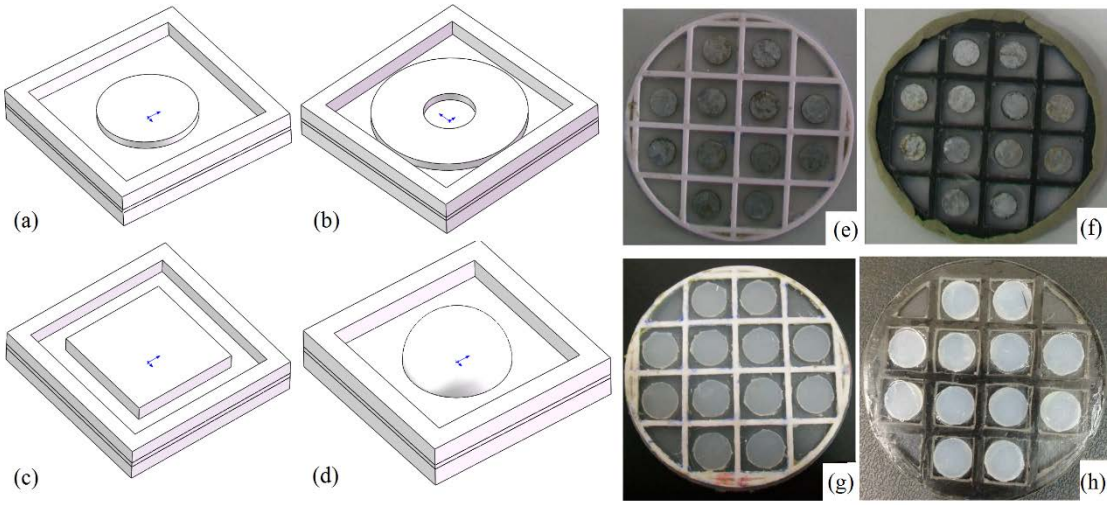

Figure 1: The plate-type unit cells with cylindrical (a), ring (b), rectangular (c) and hemispherical (d) mass blocks; some multiple cells experiment samples with different type of mass and frame (e~h).

To investigate the influences of the film thickness and the frame material on the sound insulation ability, several groups of sound transmission losses (STLs) for the two types of mass blocks (cylindrical and ring) under different film thicknesses and frames are shown in Fig. 2. For the two sets of specimens with the same ABS frames, the STL of the one with thickness of 0.5mm within 200-275Hz proved about 2dB in average higher than that of the 1mm-thick one; while within the range

above 275Hz, the 1mm-thick specimen exhibited a higher STL than that of the 0.5mm-thick one, and especially the maximum difference reached 10dB above 400Hz. For the two sets with the same film thickness of 1mm, the specimen with EVA frame exhibited a higher STL than that of the ABS one within 200-350Hz, 5dB higher in average than the control group, and the maximum difference reached up to about 12dB. While between 350Hz and 500Hz, the STL of the ABS one got higher than that of the EVA one. And when it was above 500Hz, the gain increased, which was associated with the case that EVA is higher than ABS and rubber in the density, and the higher the frame density, the better the sound insulation ability at low frequencies. The STL of the cylindrical mass specimens are shown in Fig. 2b. For the two sets of specimens with the same ABS frames, almost among the entire frequency band, the STL of the 0.5mm-thick one proved higher than that of the 1mm-thick one, with the highest difference of approximately 15dB; while only in the band between 200Hz and 300Hz, the 1mm-thick specimen exhibited a higher STL than the control group, approximately 5dB higher in average. For the two sets with the same1mm-thickness film, almost among the whole frequency band, the specimen with EVA frame exhibited a higher STL than the ABS one, with the maximum difference more than 10dB and an average difference approximately 8dB in the band above 260Hz. Overall, beyond a certain frequency, the STLs of the membrane-type acoustic metamaterials specimens proved lower than that of the control group. That is, a better sound insulation ability of this type of thin-film specimen could be exhibited only at low frequencies.

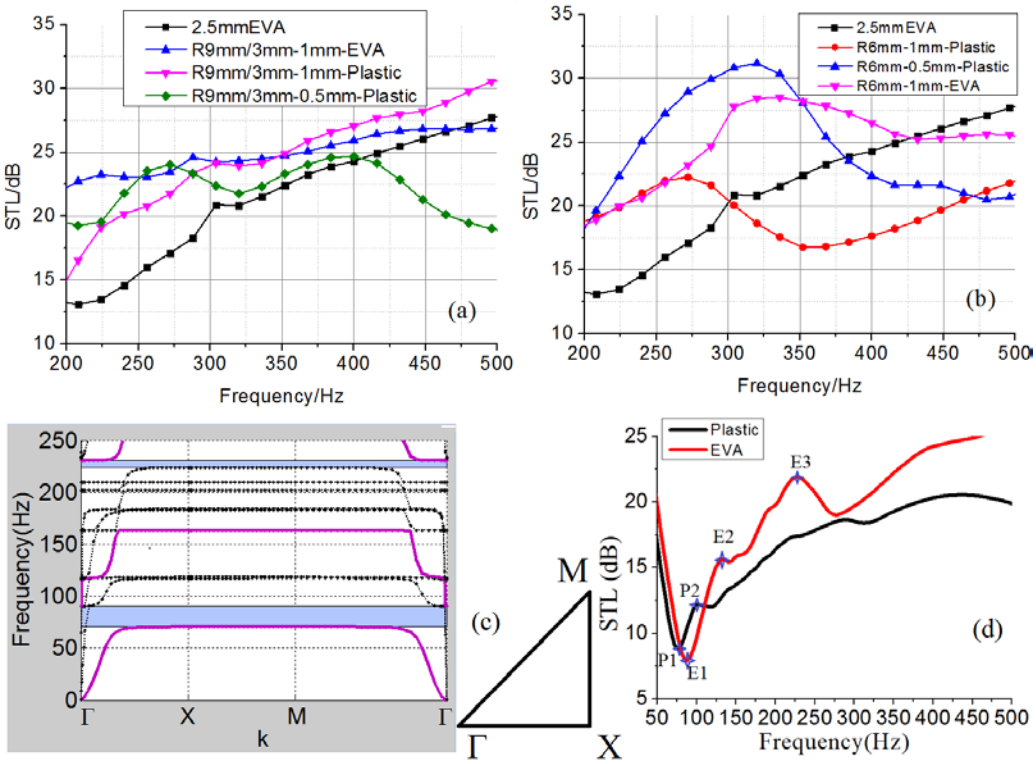

Figure 2: The STL comparing of the samples with ring (a) and cylindrical (b) mass blocks and different membrane thickness and frame type; (c) band structure of cylindrical mass unit; (d) the comparison of the STL among different samples. The first Brillouin zone is shown in the inset.

To investigate the sound attenuation mechanism and locally resonant property of the proposed structures, by using the finite element software COMSOL Multiphysics, band structure of the unit cells in Fig, 1a~d are solved, and that of the unit with cylindrical rubber mass is shown in Fig. 2c. Comparing the band structure of Fig. 2c with the measured STL results of Fig. 2d, it is suggested that in the ranges of the bending wave band gap, these results are consistent with each other. It means on the one hand, the band structure and STL calculation are validated by the experiment; one the other hand, the sound insulation ability of the proposed structure are experimentally validated. The structures proposed in this section have potential applications in the low-frequency vibration and noise

reduction. It is well known that for local resonant type structure, the periodicity is not very important, so the application range could be expand. For example, it could be fabricated with some small parts with the size of near 100×100mm, and these small parts could be located in the regions of the thin-shell part where the low-frequency vibration is most intense. This method is similar to the traditional method, which achieves the vibration and noise reduction by pasting the mass and damping blocks on the intense vibration regions. In addition to achieving the low-frequency vibration reduction and sound insulation through the local resonance characteristic of this type of structure, because this type of structure is mainly composed by rubber with large damping value, the traditional damping attenuation effect can also be realized.

3 MULTILAYER 1D PLATE-TYPE ACOUSTIC METAMATERIALS

In this section, by introducing thin air layer between plate layers and using different material and thickness parameters, we designed some kinds of multilayer 1D plate-type composite structures. For briefer description, the basic material units employed here are classified as that: A denotes the 0.1mm-thickness PET film, B the 0.2mm-thick polyamide film consisting of a 0.1mm-thickness rigid nylon film with an approximately 0.1mm-thick lightweight coating, and C the 0.5mm-thickness EVA film. All composite structures are constituted by these basic units, and the components are directly stacked on each other without any intermediate connecting material. Some samples are shown in Fig. 3a~b.

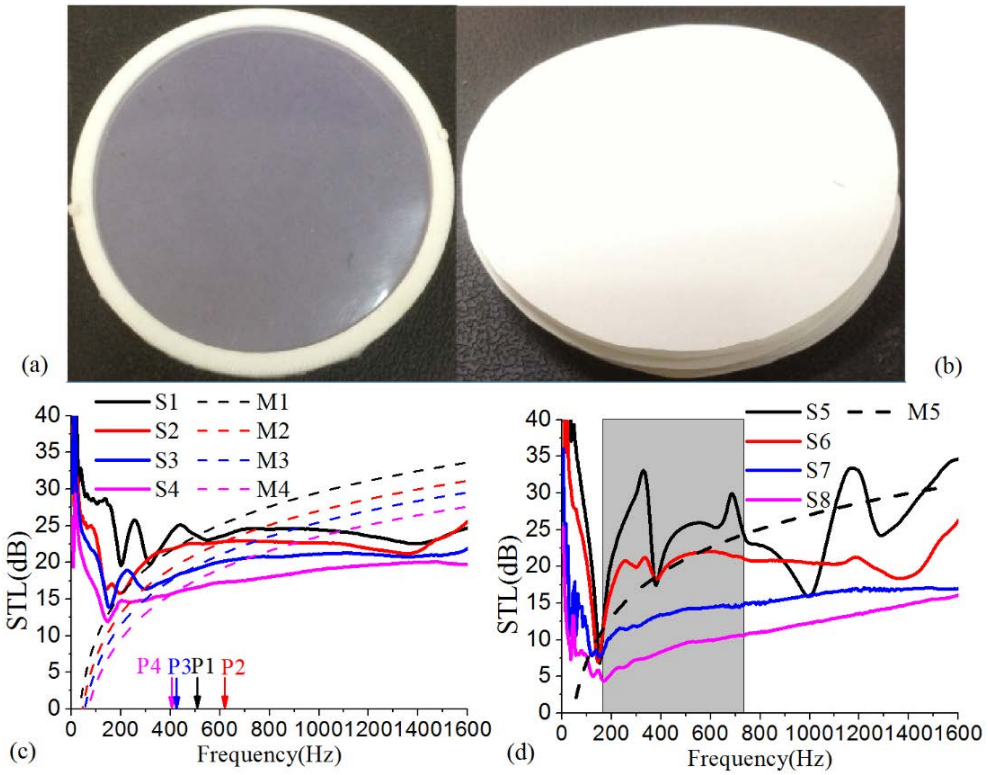

Figure 3: (a) 40-layers PET film structure (S1); (b) 20-layers polyamide film composite structure (S5); (c) The STLs comparison for PET composite film structures of 0.1mm-thickness multilayer and the corresponding results predicted by the mass density law with the same areal density, wherein, the areal density of S1 and M1 is 4kg/m^3, S2 and M2 is 3kg/m^3, S3 and M3 is 2.5kg/m^3, S4 and M4 is 2kg/m^3 respectively, meanwhile the frequency of P1 (black arrow), P2 (red arrow), P3 (blue arrow) and P4 (purple arrow) is 509Hz, 622Hz, 426Hz and 408Hz respectively; (d) the STLs comparison for polyamide composite film structures of 0.1mm-thickness multilayer and the corresponding results predicted by the mass density law with the same areal density, wherein, S5 and M5 have the areal density of 3kg/m^3, the lower edge of the shaded frequency area is 168Hz, and the upper edge is 736Hz. The structure forms: S1(40×A), S2(30×A), S3(25×A), S4(20×A), S5(20×B), S6(16×B), S7(12×B), S8(8×B), S9(CB×5), and S10(CBCBCBC).

The measured STL curves of S1~S4 are compared in Fig. 3c, wherein M1~M4 are the results predicted by the mass density law, which successively have the same areal density as S1~S4, and P1~P4 are the critical frequency points respectively when S1~S4 break the mass density law. Figure 3c suggests that the STL amplitude will increase nonlinearly with the film layers in the whole test band. However, due to the structures resonance, in the range below 600Hz the STL curves undergo large fluctuations, especially for S1, which means that the STLs of these structures depend not merely on the thickness and areal density, but also the film layers. Comparing the results predicted by the mass density law for M1~M4, it is suggested that the mass density law could be effectively broken by these 1D structures in the low frequency ranges. Moreover, in the range of 200~500Hz, the average STL amplitude of S1 is approximately 4dB higher than that predicted by the mass density law, and the largest gain reaches almost 10dB, which reflects the excellent sound insulation ability of the acoustic metamaterials in the low frequency range. The STLs of S5~S8 are compared in Fig. 3d, wherein M5 with the same areal density as S5 is the results predicted by the mass density law. The polyamide film is constituted by the nylon film with large stiffness and a layer of ultra-light coating, which results in a solid-solid composite structural form consisting of alternating materials. In the range of 168-736Hz, the mass density law can be broken by S5, the average STL amplitude of S5 is about 8dB larger than M5, and the maximum gain approaches to 18dB. After the number of layers reaches 16, the STL amplitude could always remain above 20dB, and more than 90% transmittance sound waves can be attenuated. The STL curves of 8-layers and 12-layers structures (S7 and S8) have changed smoothly, which suggests that the low frequency sound insulation capability of these 1D plate-type structures mainly depend on the structure cycles after the cycle number reaches some certain value. While for the structures with smaller cycle number, that capability mainly depends on the thickness. From Fig. 3c~3d, it can be seen that the plate-type composite structures have a typical cyclical effect. Only reaching to a certain number of cycles will prompt the low frequency sound insulation ability to arise and the mass density law to be broken.

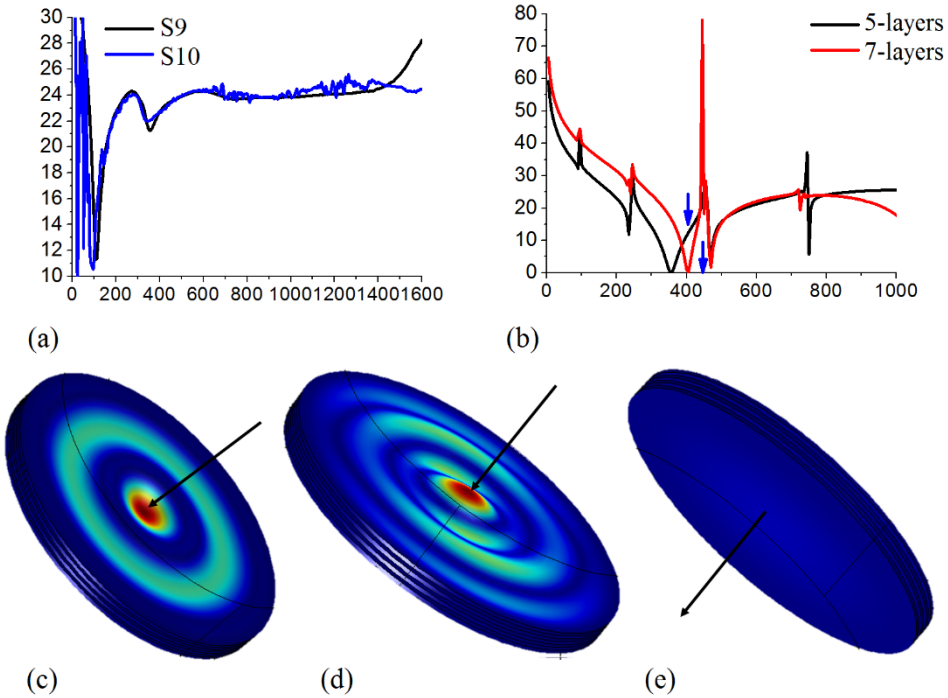

Fig. 4 The STLs comparison for (a) polyamide film and EVA film composite structures of S13 and S14; (b) the simulated STL curves of the models; the displacement contours (c~e).

In addition, although the layers of S10 are 3 less than S9 in Fig. 4a, with the sound wave incident from the same side, the STL curves almost coincide with each other, which suggests that as the film thickness increases, the surface effect of the monolayer film dominates the sound insulation and the

cyclical effect is rather weak. A possible interpretation is that the cyclical effect may have been saturated and only the surface effects may have appeared in this case. Such a feature is helpful to reduce the overall thickness and weight, as well as the cost. In theory, the trend of the STL curves of S9 and S10 in Fig. 4a should be caused by the interaction between the air layers and films. In order to reveal the physical mechanism of the saturation effect, a numerical simulation model is developed by employing the COMSOL software. Since the calculation of thinner structure is costly, we employ the 1mm-thick EVA film denoted as D, 1mm-thick nylon film denoted as E, and 1mm-thick air layer denoted as F for simulation. Composite form of the first model is DFEFD (5-layers), and that of the second model is DFEFDFE (7-layers). From the simulated STL curves in Fig. 4b it can be seen that although the total thickness of second model (7-layers) is 2mm (1mm-thick nylon film and 1mm-thick air layer) larger than the first one, the STL curves substantially coincide with each other in the range from 450 to 800Hz. In the range above 800Hz, the STL amplitudes of the first model are even larger than the second one, and such a trend qualitatively agrees with the tested one in Fig. 4a, which means that the sound insulation ability of the 1D plate-type acoustic metamaterials is mainly determined by the surface properties of the film and the interaction between the films and intermediate air layers.

The physical mechanism of the saturation effect can be further expressed by the numerical simulated displacement fields shown in Fig. 4c~e, which shows the displacement field contours of the 7-layer structure that correspond to the frequencies indicated by blue arrows. In the figures, the black arrows indicate the direction of the acoustic wave. From the left to right, the first arrow indicates the frequency of 400Hz, which corresponds to the sound insulation dip and the critical frequency of the stiffness control and damping control; while the second arrow indicates the frequency of 455Hz, which corresponds to the sound insulation peak, and the frequency point with the most obvious anti-resonant effect. From the displacement contour at 400Hz of sound insulation dip in Fig. 4c, it can be seen that the vibration direction of the structure is consistent with the sound incident direction, which leads to the maximum transmission of sound waves through the structure. And from the displacement contour at 455Hz of sound insulation peak in Fig. 4d, we can find that at this case, the vibration direction of the structure is opposite to that of the incident sound wave, and the anti-resonance effect is very obvious, so that the sound wave will be strongly reflected back by the structure. Figure 4e shows displacement contour at the back of incident sound side of the 455Hz peak frequency, we can see that at the back side, the structure almost have no vibration, which vividly shows that the periodic effect is saturated at this time, only the partial structure facing to the incident sound direction keep vibration. In fact, at other frequencies, including 400 Hz, this feature is also valid, which provides the most direct evidence for the saturation effect.

4 LUMPED MULTIPLE CELLS 2D PLATE-TYPE ACOUSTIC METAMATERIALS

In this section, by employing stiff nylon plate, several lumped multiple cells 2D plate-type acoustic metamaterials structures are designed and fabricated. The STL curves of the metamaterials samples with different frame materials and homogeneous 1.5mm-thickness EVA plate sample are experimentally measured and then compared with each other in Fig. 5a, wherein the frequencies denoted by black arrows are 234Hz, 580Hz and 1140Hz in turn, and those denoted by blue arrows are 400Hz and 963Hz, respectively. By evaluating the measured STL curves of EVA and ABS frames samples, it can be seen that in the band below 1140Hz, the STL amplitudes of the EVA frame structure are significantly greater than those of the homogeneous EVA plate. The maximum increase reaches up to 28dB at 580Hz, and the average increase get up to nearly 20dB. Even through only considering the bands above the first STL dip, i.e. the ranges above 234Hz, the maximum STL amplitude at 580Hz reaches 39dB. Because of that the STL is a logarithmic value, the STL rising to 40dB means that only 1% sound wave could transmit the structure, and 99% will be attenuated. In the range below 1000Hz, the average STL value of the metamaterials structure is close to 25dB, which implies that only less than 6% of the sound wave could transmit the structure, and the attenuation percentage reaches up to more than 94%.

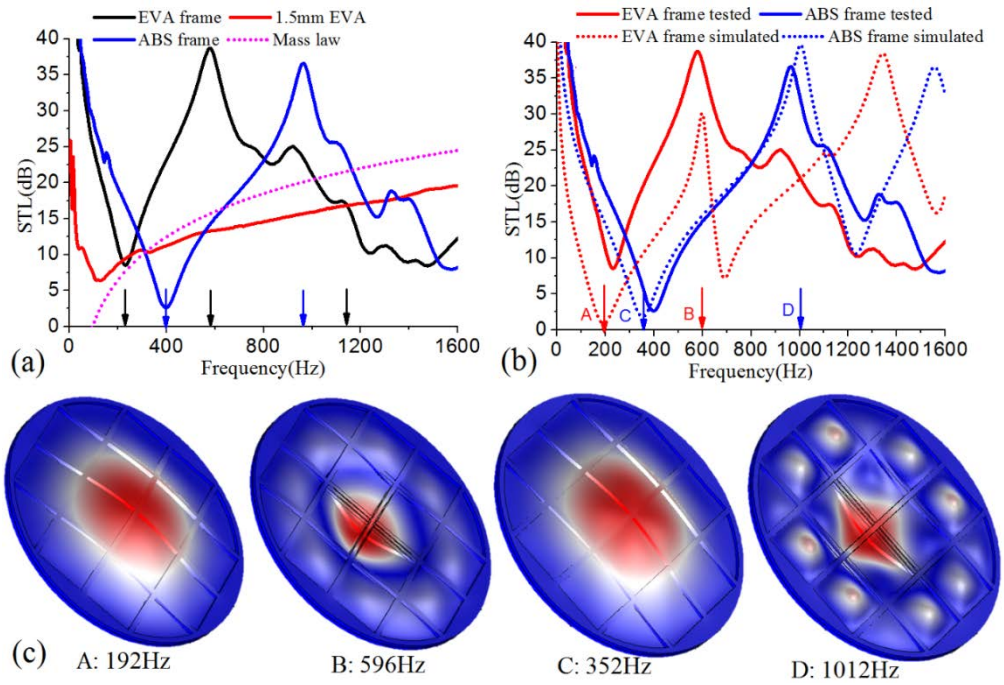

Fig. 5 (a) The measured STL curves of the metamaterials samples (both the EVA and ABS frames structures), the homogeneous 1.5mm-thickness EVA plate sample and the results predicted by the mass density law with the surface density of 1.4kg/m^2, wherein the black (blue) solid curve denotes the measured STLs of the EVA (ABS) frames structure, the red solid curve denotes the measured STLs of the EVA plate with 1.5mm-thickness, and the magenta short dot curve denotes the results predicted by the mass density law; (b) comparison of the STL curves between the measured and simulated results, wherein the red (blue) solid curve denotes the measured STL of the EVA (ABS) frames structure, and the red (blue) short dot curve denotes the simulated STLs of the EVA (ABS) frames structure; (c) the simulated vibration displacement contours in the first dip (A) and peak (B) of EVA frames sample and the first dip (C) and peak (D) of ABS frames sample.

By comparing the measured STLs of the nylon plate structures with softer EVA and stiffer ABS frames in Fig. 5a, which suggests that due to the coupling interaction between the frames and plate, the total stiffness of the sample with the EVA frames is smaller than that of the ABS frames one, and so is the coupling resonance frequency, which results in that the first dip frequency (~234Hz) of the EVA frames sample (black solid curve) is lower than that (~400Hz) of the ABS frames sample (blue solid curve). Furthermore, at the first dip frequency the STL amplitude of the EVA frames sample is approximately 6dB higher than that of the ABS frames one. Similarly, the peak frequency of the EVA frames sample is also lower than that of the ABS frames one, wherein the former is located at about 580Hz and the latter about 963Hz. Meanwhile, at each sound insulation peak frequency, the STL amplitude of the EVA frames sample is about 5dB higher than that of the ABS frames one. Due to the coupling flexural resonance between the plate and frames, the frames provide the rigidity and apply a certain additional mass to the plate through coupling with the plate, and STLs of the EVA frames structure are always greater than those of the ABS frames structure at both the first dip and peak frequencies. Since the rigidity of the EVA frame is much smaller than that of the ABS frame, the additional mass applied on the plate from EVA frames becomes larger than that from ABS frames, which leads to that the STLs of the EVA frames sample are always greater than the ABS frames one at both the dip and peak frequencies.

Figure 5b shows the measured and simulated STL curves for the structures with two types of frames, wherein the red arrows A and B denote the first dip (192Hz) and peak (596Hz) of the simulation results for EVA frames sample, respectively, close to those of the test results (234Hz and 580Hz). Meanwhile, the blue arrows C and D denote the first dip (352Hz) and peak (1012Hz) of the simulation results for ABS frames sample, respectively, close to those of the test results (400Hz and

963Hz). Overall, the calculated results are consistent with the measured results. The vibration displacement contours at the frequencies denoted by arrows A-D in Fig. 5b are shown in Fig. 5c, wherein the sound waves are all incident from the lower left side in the figures. It is shown that at the dip and peak frequencies, the lumped coupling resonant modes of the whole samples are excited. At the first dip frequencies, the vibration directions of samples are in-phase to the incident sound wave and the phases reach up to shift points, resulting in the transmitting of sound waves into the structures maximizes, which leads to the STL dips. While at the first peak frequencies, the vibration directions of samples are out-of-phase to the incident sound wave, which leads to the STL peaks and a best anti-resonance effect.

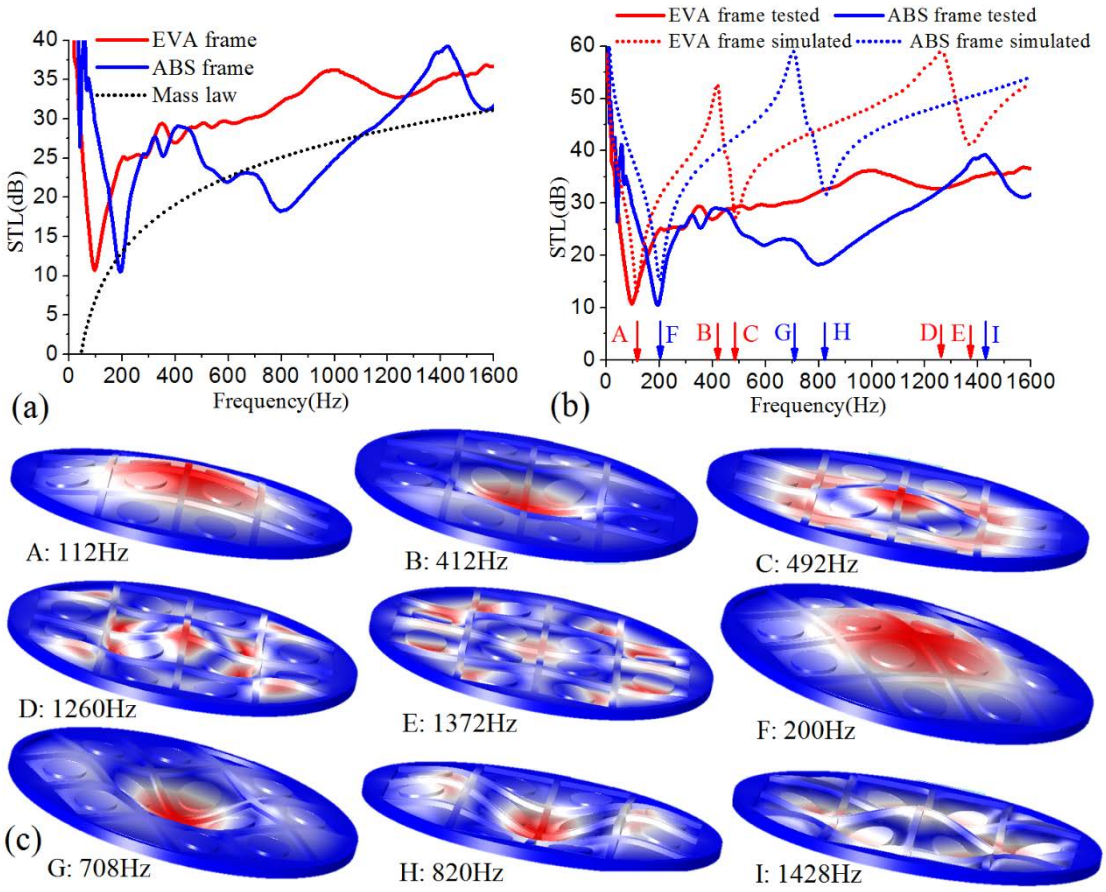

Fig. 6. (a) The measured STL curves of the metamaterials samples with mass disks (both the EVA and ABS frames structures), and the results predicted by the mass density law with the surface density of 3kg/m^2, wherein the red (blue) solid curve denotes the measured STLs of the EVA (ABS) frames structure and the black short dot curve denotes the results predicted by mass density law; (b) comparison of the STL curves between the measured and simulated results, wherein the red (blue) solid curve denotes the measured STLs of the EVA (ABS) frames structures and the red (blue) short dot curve denotes the simulated STLs of the EVA (ABS) frames structures; (c) the simulated vibration displacement contours of the point-A to point-I in Fig. 3b.

In addition, the EVA and ABS frames structures with additional mass disks are also fabricated, and the STLs are measured and numerically calculated, wherein the measured results are shown in Fig. 6a. Both surface densities of the two structures with additional masses are approximately 3kg/m2, and the results predicted by the mass density law are given in the figure as the black dot line. By comparing the measured STL curves of two different frame materials structures, it can be seen that the average STL amplitude of the EVA frames sample is approximately 10dB higher than that of the ABS frames sample in a wide frequency range of below 1250Hz, and the maximum increase reaches 15dB. Moreover, within the measure frequency band, the STL values of the EVA frames structure are always

greater than the results predicted by the mass density law, and in the frequency range above 200Hz (except the stiffness control region), the STLs of the EVA frames structure keep above 25dB and the average value is higher than 32dB, which shows excellent strong broadband sound attenuation ability.

The vibration displacement contours at the frequencies denoted by arrows A-I in Fig. 6b are shown in Fig. 6c, and the corresponding frequencies are 112Hz, 412Hz, 492Hz, 1260Hz, 1372Hz, 200Hz, 708Hz, 820Hz and 1428Hz, respectively, wherein the sound waves are uniformly incident from the lower left side in the figures. From these figures it can be seen that the EVA and ABS frames samples have similar displacement distributions. At the first dip frequencies (point-A for EVA frames structure and point-F for ABS frames structure), the vibration modes of samples both with and without additional mass disks are similar to each other, belonging to the first-order resonant mode of circular plate. In this case, the vibration directions of samples are in-phase with the incident sound wave and the phases reach up to shift points, which leads to the STL dips. At the first peak frequencies (point-B for the EVA frames structure and point-G for the ABS frames structure), the vibration modes are dominated by the anti-resonance in the center of sample, accompanied by a slight resonance in the surrounding region. Since the anti-resonance in the center is stronger than the resonance in the surrounding region, a STL peak with excellent sound insulation capability arises. For the EVA frames structure, at point-C, the center of the sample becomes in-phase resonant with the sound wave, while the surrounding region become anti-resonant. Due to that the resonance in the center is stronger than the anti-resonance in the surrounding region, a clear STL dip is produced. At point-D and point-E, vibration patterns of the lumped structure are relatively complicated for the coexistence of resonance and anti-resonance, and the STL amplitudes could be held at a high level. At the peak of point-D the STL amplitude reach up to about 60dB, and that reaches up to 40dB at the dip of point-E. Conversely, for the ABS frames structure, at point-G , the center of the sample becomes out-phase anti-resonant with the sound wave, while the surrounding region become in-phase resonant. Due to that the anti-resonance in the center is stronger than the resonance in the surrounding region, a sharp STL peak is produced. While at point-H, anti-resonance in the center is weaker than the resonance in the surrounding region, which results in a clear STL dip. In the whole frequency range above point-H, vibration patterns of the structure at different frequencies are similar to each other, i.e. the coexistence of resonance and anti-resonance, and the STL amplitude could keep a high level and increase gradually.

5 CONCLUSIONS

To sum up, for the acoustic metamaterials structural design, multilayer 1D periodic plate-type structures, 2D periodic elastic membrane and plate-type structures without tension-dependent, and the 2D plate-type structures with lumped resonance effect are presented in succession. In theory exploration, tension-dependent, local resonance theory, and the influence of the mass shape on the band structure of the 2D elastic plate-type acoustic metamaterials, the periodic effect, surface effect and saturation effect of 1D plate-type acoustic metamaterial, and lumped coupling resonance effects and the influence of the frame on sound insulation performance of the 2D plate-type acoustic metamaterials are deeply studied. The main purpose is hoping to resolve low frequency noise and vibration problems by the plate-type acoustic metamaterial in practice.

ACKNOWLEDGEMENTS

This work was supported by the National Natural Science Foundation of China (NSFC) under Grant No. 51375362.

REFERENCES

[1] Z. Yang, H. M. Dai, N. H. Chan, G. C. Ma, and P. Sheng, Acoustic metamaterial panels for sound attenuation in the 50-1000 Hz regime, Appl. Phys. Lett. 96, 041906 (2010)

[2] Y. Zhang, J. Wen, H. Zhao, D. Yu, L. Cai, and X. Wen, Sound insulation property of membrane-type acoustic metamaterials carrying different masses at adjacent cells, J. Appl. Phys. 114, 063515 (2013)

[3] J. Mei, G. Ma, M. Yang, Z. Yang, W. Wen, and P. Sheng, Dark acoustic metamaterials as super absorbers for low-frequency sound, Nature Comm. 3, 1758 (2012)

[4] Z. Liu, X. Zhang, Y. Mao, Y. Zhu, Z. Yang, C. Chan, P. Sheng, Locally resonant sonic materials, Science 289: 1734-1736 (2000)

[5] S. A. Cummer, J. Christensen and A. Alù, Controlling sound with acoustic metamaterials, Nature Rev. Mater. 1, 16001 (2016)

[6] Y. Pennec, B. Djafari-Rouhani, H. Larabi, J. O. Vasseur, and A. C. Hladky-Hennion, Low-frequency gaps in a phononic crystal constituted of cylindrical dots deposited on a thin homogeneous plate, Phys. Rev. B 78, 104105 (2008)

[7] C. Sun, J. Hsu, and T. Wu, Resonant slow modes in phononic crystal plates with periodic membranes, Appl. Phys. Lett. 97, 031902 (2010)

[8] F. Ma, J. Wu, M. Huang, G. Fu, and C. Bai, Cochlear bionic acoustic metamaterials, Appl. Phys. Lett. 105, 213702 (2014)

[9] Z. Yang, J. Mei, M. Yang, N. Chan, and P. Sheng, Membrane-type acoustic metamaterial with negative dynamic mass, Phys. Rev. Lett. 101, 204301 (2008)

[10] F. Ma, J. H. Wu, M. Huang, W. Zhang and S. Zhang, A purely flexible lightweight membrane-type acoustic metamaterial, J. Phys. D: Appl. Phys. 48, 175105 (2015)

[11] F. Ma, J. H. Wu, and M. Huang, Resonant modal group theory of membrane-type acoustical metamaterials for low-frequency sound attenuation, Eur. Phys. J. Appl. Phys. 71, 30504 (2015)

[12] G. Ma, M. Yang, S. Xiao, Z. Yang, and P. Sheng, Acoustic metasurface with hybrid resonances, Nature Matter. 13: 873-878 (2014)

[13] C. J. Naify, C. Chang, G. McKnight, and S. Nutt, Transmission loss of membrane-type acoustic metamaterials with coaxial ring masses, J. Appl. Phys. 110, 124903 (2011)

[14] Y. Chen, G. Huang, X. Zhou, G. Hu, and C. Sun, Analytical coupled vibroacoustic modeling of membrane-type acoustic metamaterials: Plate model, J. Acoust. Soc. Am. 136 (6): 2926-2934 (2014)

[15] C. J. Naify, C. Chang, G. McKnight, F. Scheulen, and S. Nutt, Membrane-type metamaterials: Transmission loss of multi-celled arrays, J. Appl. Phys. 109, 104902 (2011)

[16] M. Yang, G. Ma, Z. Yang, and P. Sheng, Coupled membranes with doubly negative mass density and bulk modulus, Phys. Rev. Lett. 110, 134301 (2013)

[17] Y. Chen, G. Huang, X. Zhou, G. Hu, and C. Sun, Analytical coupled vibroacoustic modeling of membrane-type acoustic metamaterials: Membrane model, J. Acoust. Soc. Am. 136 (3): 969-979 (2014)

[18] F. Ma, J. H. Wu, M. Huang, and S. Zhang. Cochlear outer hair cell bio-inspired metamaterial with negative effective parameters, Appl. Phys. A 122, 525 (2016)

[19] F. Ma, J. H. Wu and M. Huang, One-dimensional stiff film acoustic metamaterials, J. Phys. D: Appl. Phys. 48, 465305 (2015)

[20] T. Huang, C. Shen, and Y. Jing, Membrane- and plate-type acoustic metamaterials, J. Acoust. Soc. Am. 139 (6): 3240-3250 (2016)

[21] F. Ma, J. H. Wu, and M. Huang, Ultrathin lightweight plate-type acoustic metamaterials with positive lumped coupling resonant, J. Appl. Phys. 121, 015102 (2017).